Applied Energy 377 (2025) 124609

Contents lists available at ScienceDirect

Applied Energy

journal homepage: www.elsevier.com/locate/apenergy

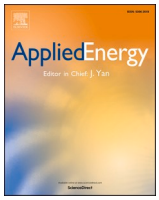

# An efficient ordered conversion system for hydrogen and electricity cogeneration driven by concentrated solar energy

Entao Zhang, Chenyu Xu *, Yuan Gao, Xuan Zhu, Yin Xie, Mingpan Xu, Yanwei Zhang *

*State Key Laboratory of Clean Energy Utilization, Zhejiang University, Hangzhou 310027, China*

## HIGHLIGHTS

- A novel ordered conversion system for hydrogen and electricity cogeneration.
- The dissipated heat of EHPs could be efficiently reutilized.
- The system exergy efficiency could be improved to 28.49 %.
- Exergy efficiency was adjusted by photocatalytic temperature based on DNI.

## GRAPHICAL ABSTRACT

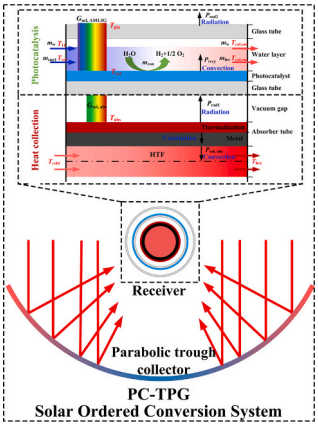


## ARTICLE INFO

*Keywords:*
Solar energy
Ordered conversion
Hydrogen-electricity cogeneration
Full-spectrum

## ABSTRACT

Efficient utilization of full-spectrum solar photons is significant for improving the efficiency of solar energy conversion and thus alleviating energy shortage. In this work, a novel concentrated ordered conversion system based on a parabolic trough collector (PTC) that couples photocatalysis and Rankine cycle for hydrogen and electricity cogeneration to more efficiently use the full-spectrum solar energy is proposed. Higher-energy photons are absorbed by the photocatalytic layer for water splitting hydrogen production, and the remaining photons with lower energy that cannot excite electron-hole pairs (EHPs) are transmitted to the photocatalytic layer and converted into thermal energy to drive the Rankine cycle for electricity generation. Furthermore, the EHPs dissipated heat and absorber tube radiation heat loss can be reutilized in the photocatalytic layer to preheat the circulating water to increase the reaction temperature and solar evaporator inlet temperature to the designate temperature of 140 °C. Solar photocatalysis model and thermodynamic model are developed to simulate and analyze the system performance. Of the input solar energy, 10.34 % and 17.85 % are converted into hydrogen and electricity by photocatalysis and Rankine cycle processes, respectively. The total exergy efficiency increases from 23.51 % for the conventional PTC thermal power generation system to 28.49 % for the proposed system under the design condition. Then, the effects of the photocatalyst bandgap and temperature on the system exergy efficiency are analyzed, which indicates that when the photocatalyst bandgap increases, its operating

* Corresponding author.
*E-mail addresses:* mrxcy@zju.edu.cn (C. Xu), zhangyw@zju.edu.cn (Y. Zhang).

https://doi.org/10.1016/j.apenergy.2024.124609
Received 4 June 2024; Received in revised form 14 September 2024; Accepted 27 September 2024
Available online 8 October 2024

temperature should be adjusted downward. The photocatalytic layer temperature is adjusted for corresponding maximum system exergy efficiency under different direct nominal irradiation (DNI) conditions, and it can maintain 140 °C of operation when DNI is greater than 240 W·m$^{-2}$. This research provides a new approach to improve the efficiency and flexibility of full-spectrum solar utilization.

**Nomenclature**

| | |
|---|---|
| $A$ | area, m$^2$ |
| c | lightspeed, m·s$^{-1}$ |
| $c$ | specific heat capacity, J·kg$^{-1}$·°C$^{-1}$ |
| $E$ | energy, J |
| $Ex$ | exergy, J |
| $F$ | generation and recombination rate of EHPs, s$^{-1}$ |
| $\Delta G$ | Gibbs free energy, J·mol$^{-1}$ |
| h | Planck constant, J·s |
| $h$ | specific enthalpy, kJ·kg$^{-1}$ |
| $H$ | enthalpy, kJ |
| $I$ | the surface reaction current, A |
| k | Boltzmann constant, J·K$^{-1}$ |

*Subscripts*

| | |
|---|---|
| abs | the absorber tube |
| ave. | the average value |
| c | cutoff |
| cat | the catalyst layer |
| che | chemical |
| cold | cold tank |
| cons | consumption |
| d | design |
| ele | electricity |
| eva | evaporator |
| ex | exergy |
| G | generator |
| g | gap |
| gla | glass tube |
| hot | hot tank |
| hyd | hydrogen |
| i | state point |

*Abbreviations*

| | |
|---|---|
| CR | conventional receiver |
| EHPs | electron-hole pairs |
| DNI | direct nominal irradiation |
| HPT | high pressure turbine |
| LPT | low pressure turbine |
| NPCW | non-preheating the circulating water |

*Greek Symbols*

| | |
|---|---|
| α | transmissivity |
| β | mass flow distribution ratio |
| γ | reflectivity |
| δ | limiting magnitude of *T-S* slope |
| $\varepsilon$ | emittance |
| $\eta$ | efficiency |
| $m$ | mass flow rate, kg·s$^{-1}$ |
| $M$ | mass, kg |
| $n/p$ | concentrations of electron and hole |
| $N$ | solar concentration ratio |
| $P$ | power, W |
| $Q$ | heat, J |
| $s$ | specific entropy, kJ·kg$^{-1}$·°C$^{-1}$ |
| $S$ | entropy, kJ·°C$^{-1}$ |
| $t$ | probability of generating EHPs |
| $T$ | temperature, °C |
| $\Delta T$ | temperature difference, °C |
| $V$ | the potential energy of EHPs, V |
| in | inlet |
| ise | isentropic |
| m | mechanical |
| mo | motor |
| non-rad | non-radiative recombination |
| out | outlet |
| p | pressure |
| pp. | pinch point |
| rad | radiative recombination |
| ref. | reference point |
| reh | reheater |
| relax | relaxation |
| sol | solar |
| th | thermal |
| T | turbine |
| w | water |
| PCW | preheating the circulating water |
| PC-TPG | photocatalysis-thermal power generation |
| PR | proposed receiver |
| PTC | parabolic trough collector |
| SM | solar multiple |
| TES | thermal energy storage |
| Θ | average phonon temperature, K |
| $\mu$ | ratio related with degree of phonon dispersion, eV·K$^{-1}$ |
| $\lambda$ | wavelength, nm |
| $\rho$ | absorptance |
| σ | Stefan-Boltzmann constant, W·m$^{-2}$·K$^{-4}$ |
| $\tau$ | time step, h |

## 1. Introduction

The sustainable development of society is facing the energy shortage problem, and energy transformation has become the primary common global issue [1,2]. Among all the available energy sources, solar energy is abundant, environmentally friendly, and can largely alleviate the tight energy supply in the world and optimize the energy structure [3]. Light utilization and thermal utilization are two main approaches for utilizing solar energy [4]. Light utilization mainly refers to the conversion of photons into electrons, after which they are directly utilized, e.g., in solar cells and photochemistry. In contrast, thermal utilization refers to the conversion of photons into electrons, which are converted into thermal energy through electron–phonon scattering and phonon–phonon scattering, thus increasing the temperature of the system and finally converting solar energy into thermal energy. According to the quality and utilization method of thermal energy, it can be classified into thermal power generation, thermochemistry, etc.

However, according to thermodynamic analysis, the quality of solar photon energy differs at different wavelengths [5]. The high-energy photons for photochemical [6] reactions or photovoltaics [7] have superior efficiencies to thermal utilization. However, the light utilization

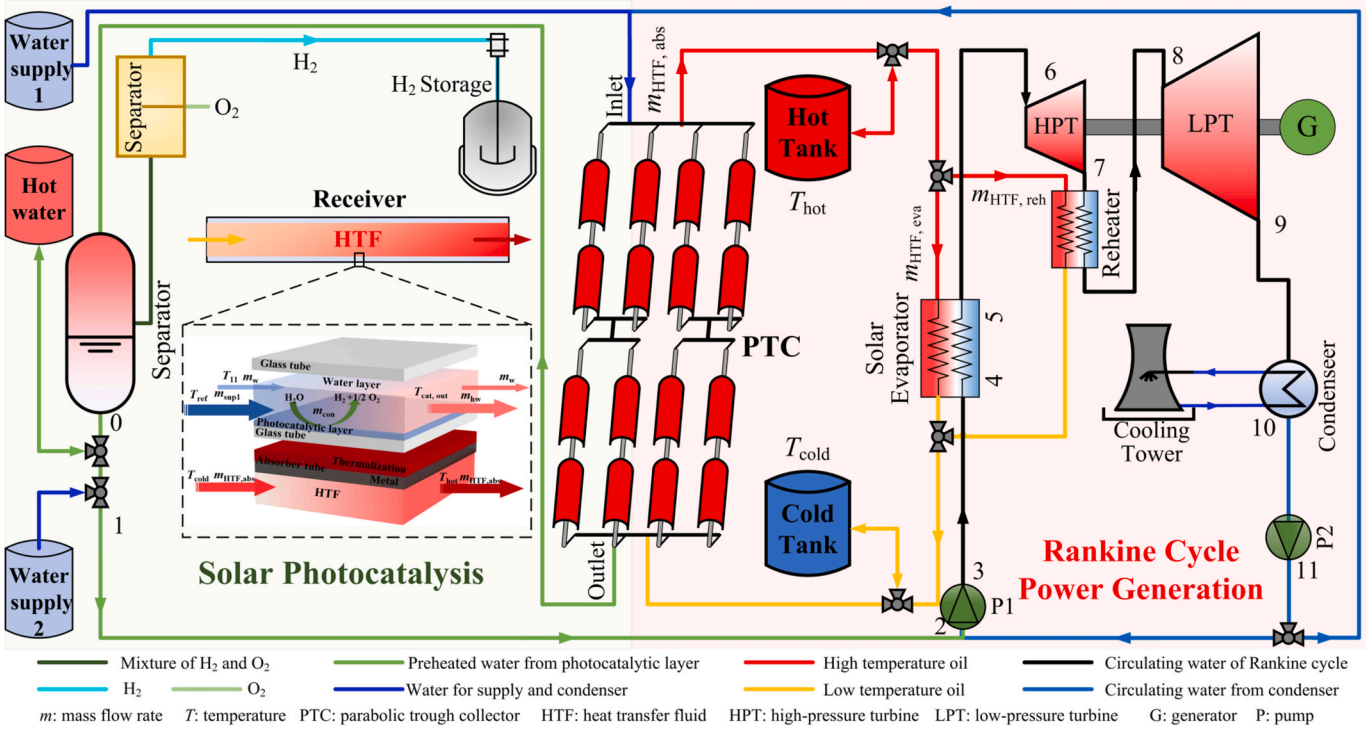


**Fig. 1.** Schematic diagram of the proposed PC-TPG hybrid system.

efficiency is limited by the semiconductor bandgap [8]. For a given semiconductor, there is a theoretical limiting efficiency due to the imperfect matching between the photon energies in the full solar spectrum and the bandgap [9]. Although the thermal utilization process can utilize solar energy across the full spectrum, the difference in the quality of photons at different wavelengths is not accounted for, resulting in a very large and irreversible loss of high-energy photons. Thus, a solar ordered conversion system could be designed to improve the solar energy utilization efficiency by integrating light and thermal utilization processes. In recent years, many researchers have focused on the full-spectrum solar energy conversion system which can be divided into two main categories: photovoltaic-thermal and photochemical-thermal. Higher-energy photons are directly converted into electrical or chemical energy, and lower-energy photons are converted into heat.

For photovoltaic-thermal system, photovoltaic layer and heat collection layer usually tends to be tandem structures. One issue is that higher temperature of heat collection layer can increase the recombination rate of electron-hole pairs (EHPs), which reduces the solar cell efficiency. Thus, tandem structure of photovoltaic-thermal system typically has lower collecting temperatures, and the lower temperature heat utilization mainly involves the generation of clean water [10], space heating [11], etc. Otherwise, spectral beam splitting technology in photovoltaic-thermal system is a promising approach which allows for the separation of electrical energy generation and heat collection [12]. It can avoid the negative effects of higher temperatures on solar cells and achieve full-spectrum solar conversion [13]. Furthermore, the higher the heat collection temperature, the lower the irreversible losses in the solar energy conversion process [14]. However, this technology will generate dissipated heat through non-radiative recombination and relaxation of EHPs which is transferred to cooling water and cannot be reutilized by the photovoltaic-thermal system [15]. Besides, it often requires expensive beam-splitting devices, which limits its value for large-scale applications. Above all, it is of great significance to establish a full-spectrum solar energy conversion system which has the functions of spectral beam splitting, dissipated heat reutilized, and obtaining high temperature heat energy simultaneously.

For photochemical-thermal system, it can directly utilize internally generated photogenerated EHPs to drive chemical reactions [16]. The dissipated heat from relaxation and non-radiative recombination of EHPs can be transferred to the reactants to increase the reaction temperature [17], which is different from photovoltaic-thermal system. At this point, raising the system temperature no longer only has the negative impact on EHPs recombination, but also accelerates the chemical reaction thermodynamics and increases the reaction rate. Film and powder of catalyst are two main types of in photochemical reaction. In powder based photochemical-thermal system, the photons which are not absorbed by the catalyst tend to be refracted or absorbed by the reactants [18], thus lowering the heat collection temperature and photon utilization efficiency. Generally, a photochemical film tends to have better transmittance and a faster reaction rate than powder [19]. In addition, photons with an energy lower than the bandgap can easily transmitted through the photochemical layer and converted into thermal energy. The thermal energy can be collected and utilized by a thermoelectric device [20], thermochemical cycles [21] or a thermal power generation system [22] according to the temperature.

In this work, firstly, based on the efficient full-spectrum utilization of solar photons, a photocatalytic film with spectral beam splitting function is combined with the conventional parabolic trough collector (PTC). Secondly, the dissipated heat generated by EHPs as well as the radiation loss from the absorber tube are fully reutilized from the perspective of thermal management. In detail, photocatalytic water splitting and the steam Rankine cycle are coupled to develop a new photocatalysis-

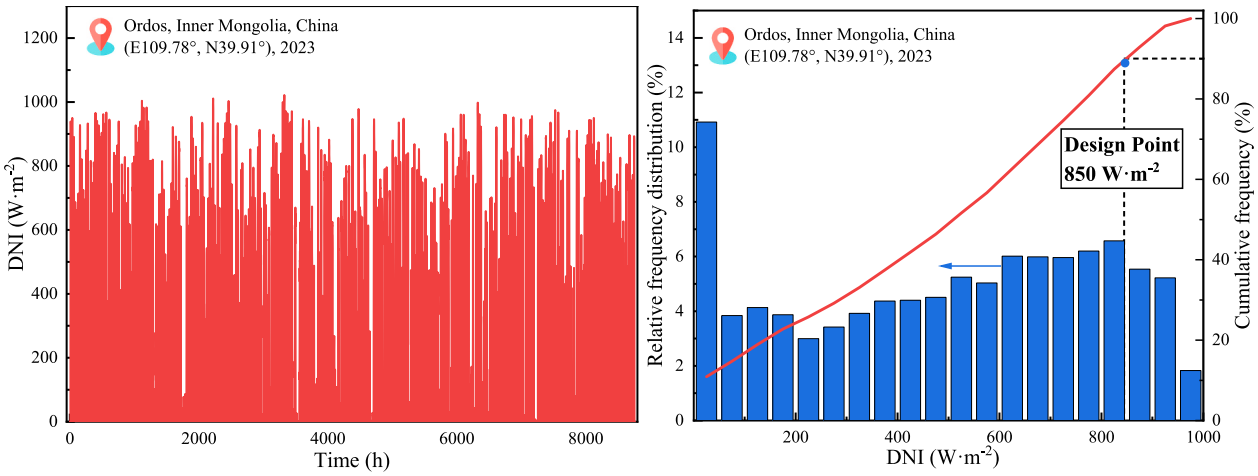


**Fig. 2.** Meteorological statistical data for 2023 with (a) annual DNI and (b) relative frequency distribution and cumulative frequency of DNI.

**Table 1**
Operational assumptions of the proposed system.

| | Parameters | Value |
|---|---|---|
| Solar collector | Solar collector aperture area ($m^2$) | 329,495 |
| | Reflectivity of the parabolic trough mirror | 0.93 [5] |
| | Aperture width of the parabolic trough mirror (m) | 5.76 |
| | Length of the PC-TPG receiver (m) | 4 |
| | Diameter of the absorber tube (m) | 0.07 |
| | Diameter of the photocatalyst tube (m) | 0.115 |
| | Diameter of the glass tube (m) | 0.15 |
| | Emittance of glass tube | 0.89 [25] |
| | Emittance of absorber tube | 0.14 |
| | Absorptance of the absorber tube | 0.96 [26] |
| | Transmissivity of the glass tube | 0.96 [25] |
| Heat storage | Temperature of hot/ cold tank (°C) | 393/ 293 [24] |
| | Storage duration (h) | 6 |
| | HTF specific heat capacity ($J·kg^{-1}·°C^{-1}$) | 2319 [27] |
| Photocatalysis | Water splitting standard Gibbs energy ($J·mol^{-1}$) | 237,130 [28] |
| | Probability of EHP generated by incident photon | 0.9 [9] |
| | $H_2O$ standard molar enthalpy of formation ($J·mol^{-1}$) | −285,800 |
| | $H_2$/ $O_2$ standard molar enthalpy of formation ($J·mol^{-1}$) | 0 |
| | $H_2O$ standard molar entropy($J·mol^{-1}·K^{-1}$) | 70 |
| | $H_2$ standard molar entropy($J·mol^{-1}·K^{-1}$) | 131 |
| | $O_2$ standard molar entropy($J·mol^{-1}·K^{-1}$) | 205 |
| Rankine cycle | Inlet pressure of high-pressure turbine (kPa) | 4000 [29] |
| | Outlet pressure of high-pressure turbine (kPa) | 1000 [29] |
| | Outlet pressure of low-pressure turbine (kPa) | 7.4 |
| | Pinch point temperature in solar evaporator (°C) | 10 [30] |
| | Pinch point temperature in condenser (°C) | 5 [31] |
| | Pinch point temperature in semiconductor surface (°C) | 5 |
| | Isentropic efficiency of HPT/ LPT (%) | 85 [29] |
| | Isentropic efficiency of water pump (%) | 75 [27] |
| | Generator efficiency (%) | 97 [32] |
| | Mechanical efficiency (%) | 98 [31] |
| | Motor efficiency (%) | 75 [27] |

thermal power generation (PC-TPG) hybrid system for hydrogen and electricity cogeneration. The photocatalytic layer acting as a natural light splitter, a radiation shield and a heat source for preheating the circulating water of Rankine cycle to the appropriate temperature. And this temperature increases benefits both the photocatalysis and Rankine cycle processes. Generally, the exergy efficiency of the proposed system increases compared to that of the conventional PTC thermal power system, from 23.51 % to 28.49 %. Furthermore, the photocatalytic layer temperature of the proposed system is adjusted for corresponding maximum system exergy efficiency under different DNI conditions. Finally, the annual performance of the system is analyzed, and the annual average exergy efficiency reaches 27.67 %.

## 2. System description and operation

### 2.1. System description

According to the photon quality, photocatalysis and the steam Rankine cycle are coupled to develop a new PC-TPG hybrid system with full-spectrum solar utilization in this work, as shown in Fig. 1. The system includes a photocatalysis (PC) process, a thermal energy storage (TES) process, a steam Rankine cycle power generation process, vapor separation and a hydrogen storage process.

First, solar radiation is directly concentrated by double-axis tracking PTCs. Then, the concentrated solar radiation passes through the glass tube and water layer in an orderly manner. Afterward, the radiation is absorbed by the photocatalytic layer, in which EHPs can be excited by solar photons and migrate to the surface of the photocatalyst for hydrogen production in the water splitting redox reaction. Finally, solar energy is converted into chemical energy and stored in chemical bonds. During the solar energy conversion, dissipated heat losses cannot be avoided. The non-radiative recombination and relaxation of EHPs are the main sources of dissipated heat in photocatalysis, which can be efficiently used to preheat feedwater through heat convection and reutilized by the Rankine cycle power generation process. Moreover, the increase in the feedwater temperature accelerates the water splitting reaction rate. In this work, to ensure that the water preheated by the photocatalytic layer can be re-pressurized by pump 2 (P2), the water splitting is set to a liquid-phase reaction. Additionally, the remaining photons with lower energy that cannot excite EHPs are transmitted through the photocatalytic layer and converted into thermal energy in the heat transfer fluid (HTF) in the absorber tube. A part of the high-temperature HTF heated by the collector is stored in the hot tank of the TES process, and the remaining part is input into the solar evaporator to drive the Rankine cycle.

Preheated water (state 0) and non-preheated water (state 11) are mixed, compressed by pump 1 (P1) and heated to a superheated vapor by a solar evaporator (processes 2 → 6) in an orderly manner. Then, the superheated vapor enters the high-pressure turbine (HPT), reheater, low-pressure turbine (LPT) and condenser in turn (processes 6 → 10) to produce power. Considering the pressure resistance of the glass tube, the circulating water is not directly pressurized to the evaporation pressure

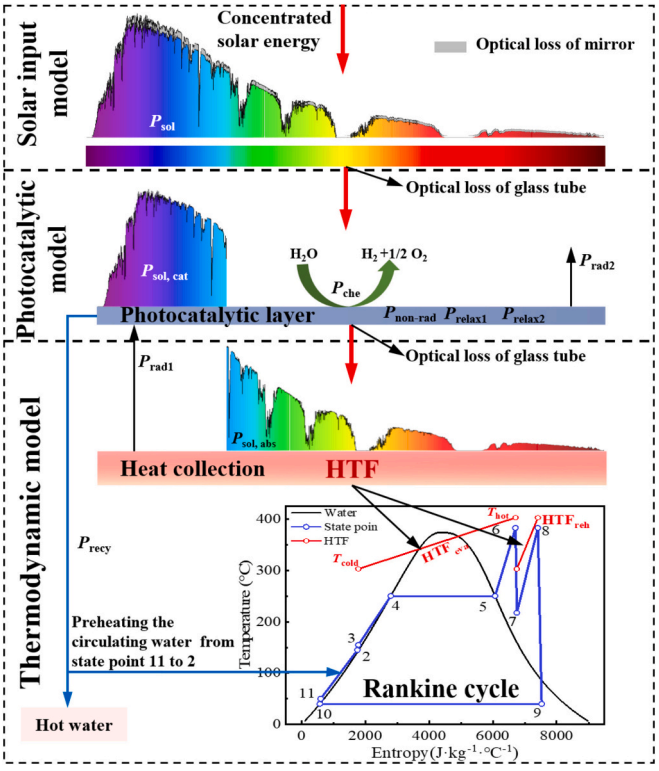


**Fig. 3.** Schematic chart for the energy flow.

of the solar evaporator through pump 2 in the proposed system. To increase the reaction temperature, improve the preheating effect and avoid optical refractive loss caused by bubbles, the circulating water needs to be pre-pressurized by P2 to increase the saturation temperature and maintain the liquid-phase reaction. A hot water tank and water supply tanks 1 and 2 are added to the proposed system. Therefore, the heat from the photocatalytic layer can be fully utilized and well stored, and the mass flow rate of the Rankine cycle can be stable.

### 2.2. System operation

In this work, the abundant solar energy in Ordos, Inner Mongolia, China (E109.78°, N39.91°) is referenced. The data of full-year hourly solar DNI is obtained from Meteonorm software, as shown in Fig. 2 (a). The relative frequency distribution of the DNI data during the solar irradiation time when DNI > 0 and the corresponding cumulative frequency, are useful to select the DNI design point [23]. And the DNI corresponding to 90 % of the cumulative frequency value is usually considered to be the design point [24]. This method of selecting design point is used in this work. Thus, the DNI design point is set at 850 W·m$^{-2}$, as shown in Fig. 2 (b). The design operating parameters of the system are shown in detail in Table 1.

## 3. Modeling

As shown in Fig. 3, the concentrated solar energy is the input energy of the system, and the photocatalysis process involves overall water splitting for hydrogen production, while the power generation process involves the steam Rankine cycle. Solar photons are absorbed by the photocatalysis process and heat collection process in turn. In this system, photons whose energy is less than the bandgap are transmitted through the photocatalytic layer. Generally, the full-spectrum solar photons can be utilized more efficiently. Besides, the proposed system achieves cogeneration of electricity, hydrogen and hot water. Following system models can be divided into four main parts. For better modeling of each energy process, solar input model, photocatalytic model and thermodynamic model are developed, as shown in Fig. 3. For better evaluating system performance, system evaluation model is developed. The performance of the catalyst is stable, and the quantum yield efficiency is set to 1. In addition, the pressure and heat losses in pipes and connections are neglected. The calculation flow chart for the system is shown in Fig. 4.

### 3.1. Solar input model

The solar energy input for the system is

$$P_{sol} = DNI \cdot A_c \tag{1}$$

where $DNI$ is direct normal irradiance; $A_c$ is solar collector aperture.

### 3.2. Solar photocatalytic model

The solar energy absorbed by the photocatalytic layer, which is related to the cutoff wavelength, can be calculated based on the AM1.5G spectrum:

$$P_{sol,cat} = A_{cat} \cdot N_{cat} \cdot \int_0^{\lambda_c} E_{sol}(\lambda)\, d\lambda \cdot \gamma \cdot \alpha_{gla} \tag{2}$$

where $A_{cat}$, $N_{cat}$ are the area and the concentration ratio of the catalyst layer, respectively. $E_{sol}$ is photon energy in specific wavelength, $\rho_c$ is the cut-off wavelength of the catalyst, γ is the reflectivity of the mirror and $\alpha_{gla}$ is the transmissivity of the glass tube.

The decay processes include relaxation, radiative recombination and non-radiative recombination [33]. All these decay processes will result in energy loss and electron potential energy loss based on the Shockley model [9]. Only the EHPs that successfully migrate to the semiconductor surface contribute to photocatalysis. In this work, the detailed balance model proposed by Shockley is used. The carrier balance equation inside the semiconductor is shown in Eq.(3):.

$$F_{sol}\left(E_g(T_{cat})\right) - F_{rad}(T_{cat}) - F_{non\text{-}rad}(T_{cat}) - I_{cat}(T_{cat})/q = 0 \tag{3}$$

where $F_{sol}$, $F_{rad}$ and $F_{non\text{-}rad}$ stand the generation rate of EHPs, the radiative recombination rate, and the non-radiative recombination rate, respectively. $I_{cat}$ is photocatalytic reaction current, $E_g$ is the catalyst band gap, $T_{cat}$ is the catalyst surface temperature and $q$ is the electronic charge.

Temperature affects the bandgap of a semiconductor, which affects its light absorption property; therefore, the four-parameter empirical equation for the temperature dependence of the bandgap proposed by Passler is adopted [34].

$$E_g(T_{cat}) = E_g(0) - \frac{\Theta\delta}{2}\left[\sqrt[\mu]{1+\left(\frac{2T_{cat}}{\Theta}\right)^{\mu}} - 1\right] \tag{4}$$

where Θ stands the average phonon temperature, δ is the limiting magnitude of temperature entropy slope which is set to 2.6, and $\mu$ is the ratio related with degree of phonon dispersion which is set to $3{\cdot}10^{-4}$ eV·K$^{-1}$.

The generation rate of EHPs can be calculated:

$$F_s = A_{cat} \cdot t_{sol} \cdot N_{cat} \cdot \int_0^{\lambda_c} \lambda \cdot \frac{E_s(\lambda)}{hc}\, d\lambda \tag{5}$$

where $t_{sol}$ is the probability of EHPs generated by incident photon, h and c are the Planck constant and light speed, respectively.

Electrons produced by high-energy photons relax to the bottom of the conduction band, and the time scale ranges from 1 to 100 ps [35]. The electron energy is converted into the vibrational energy of lattice atoms and finally converted into heat through electron–phonon interactions [33]. The relaxation energy can be calculated by:

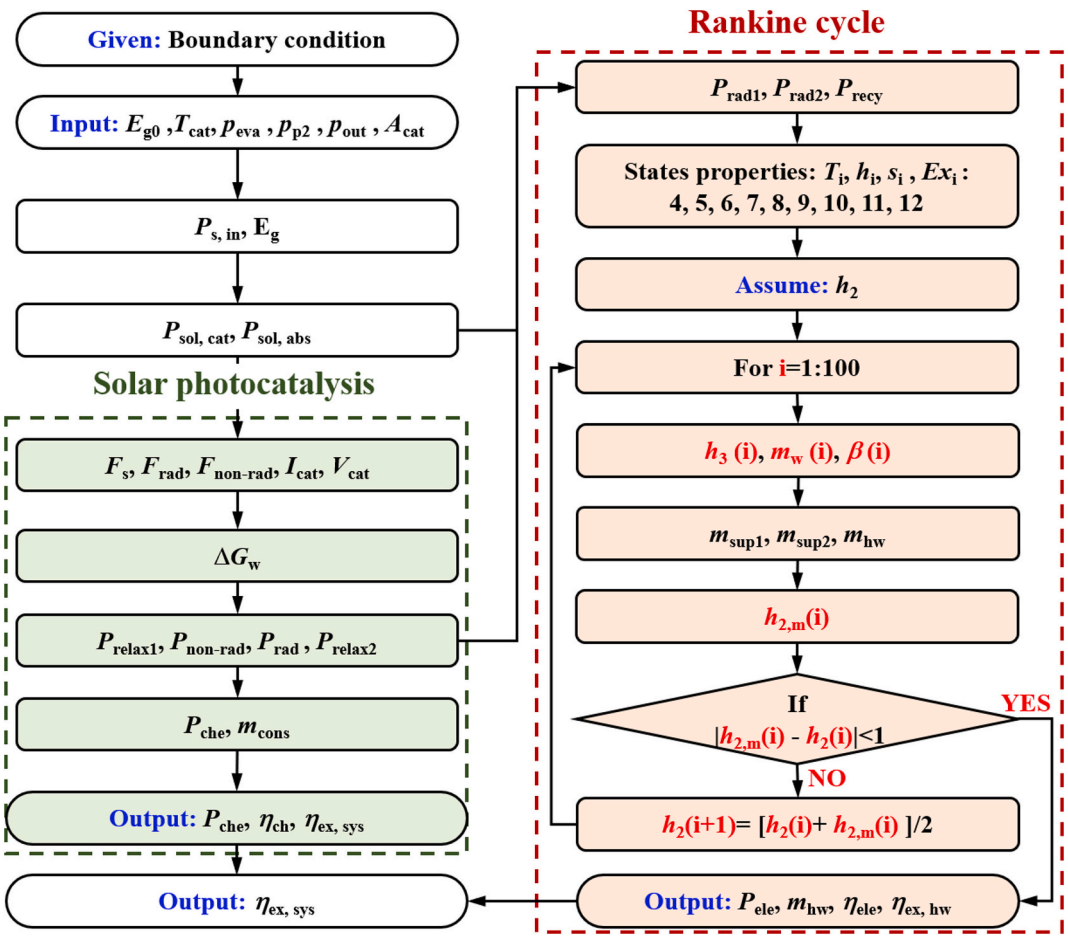


**Fig. 4.** The calculation flowchart for the proposed system.

$$P_{relax1} = A_{cat}\cdot t_{sol}\cdot N_{cat}\cdot \int_0^{\lambda_c} \left[E_s(\lambda) - E_g\right] d\lambda \tag{6}$$

The recombination types in a catalyst are mainly divided into radiative and non-radiative recombination. In radiative recombination, energy is released in the form of light, which is mainly related to the concentration of EHPs. Photoexcitation of carriers causes splitting of the Fermi energy level and generates a potential difference $V$, which could drive water splitting. Therefore, the radiative recombination rate can be expressed:

$$F_{rad} = F_{eq}\cdot\frac{n_{sol}\cdot p_{sol}}{n_0\cdot p_0} = F_{eq}\cdot exp\left(\frac{V_{cat}q}{kT_{cat}}\right) \tag{7}$$

where $F_{eq}$ is the radiative recombination rate in thermal equilibrium. $n_{sol}$ and $p_{sol}$ are the electron and the hole concentration after photon excitation, while $n_0$ and $p_0$ are the electron and the hole concentration in thermal equilibrium, respectively, $V_{cat}$ is the potential energy of EHPs.

The radiative recombination rate in thermal equilibrium condition is mainly related to the temperature and could be calculated:

$$F_{eq} = 2\pi A_{cat} c t_{cat} \int_0^{\lambda_c} \left(e^{\frac{hc}{\lambda kT_{cat}}} - 1\right)^{-1}\cdot\lambda^{-4} d\lambda \tag{8}$$

where $t_{cat}$ is the probability of EHPs generated by the environment of catalyst temperature, $k$ is the Boltzmann constant.

EHPs are destroyed through non-radiative recombination, and energy is released in the form of heat. The non-radiative recombination rate can be calculated by assuming the fraction coefficient $f$:

$$F_{non-rad} = F_{eq}\cdot\frac{1-f}{f}\cdot exp\left(\frac{V_{cat}q}{kT_{cat}}\right) \tag{9}$$

The non-radiative recombination energy can be calculated by:

$$P_{non-rad} = F_{non-rad}\cdot E_g \tag{10}$$

The relaxation and non-radiative recombination of EHPs and radiation heat transfer from the absorber tube provide a steady heat flux to the photocatalytic layer, which is used to increase the reaction temperature. Thus, the Gibbs free energy for water splitting is changed, and the oxygen and hydrogen temperatures are not the same as the initial temperature. The Gibbs free energy can be calculated:

$$\Delta G(T_{hw,ave}) = \mu_{H_2}(T_{hw,ave}) + \frac{1}{2}\mu_{O_2}(T_{hw,ave}) - \mu_{H_2O}(T_{11}) \tag{11}$$

where $\mu_i$ represents the chemical potential of component $i$, $T_{hw,ave}$ is the average temperature of the water flowing through the catalytic layer, which is set as the mean value of inlet and outlet temperatures, $T_{11}$ is the outlet temperature of P2.

The chemical potential of oxygen and hydrogen is calculated by:

$$\begin{aligned}\mu_i(T_{hw,ave}) = &\left[\Delta H_{ref,i} + H_i(T_{hw,ave}) - H_i(T_{11})\right] \\ &- T_{hw,ave}\left[\Delta S_{ref,i} + S_i(T_{hw,ave}) - S_i(T_{11})\right]\end{aligned} \tag{12}$$

where $\Delta H_{ref}$, $\Delta S_{ref}$ are the standard molar enthalpy of formation and entropy, $H$, $S$ are the enthalpy and entropy at specific temperature states, respectively. $i$ represents the component of oxygen and hydrogen.

The chemical potential of water is calculated by:

$$\mu_{H_2O}(T_{11}) = \left[\Delta H_{ref,H_2O} + H_i(T_{11}) - H_i(T_{ref})\right] - T_{11}\left[\Delta S_{ref,H_2O} + S_i(T_{11}) - S_i(T_{ref})\right] \quad (13)$$

In the water splitting reaction, the potential of the conduction band edge should be more negative than the water reduction potential, while the valence band edge should be more positive than the water oxidation potential. Electronic energy greater than the potential difference of water splitting will be released as heat energy through relaxation. The relaxation energy in the process of surface reaction can be calculated by:

$$P_{relax2} = \frac{I_{cat}}{q}\left[E_g - \frac{1000 \cdot \Delta G}{2 \times 6.02 \times 10^{23}}\right] \quad (14)$$

Part of the circulating water flowing through the photocatalytic layer will split into oxygen and hydrogen, and the mass flow rate of the consumed water is:

$$m_{cons} = \frac{I_{cat}}{2 \times 1000 \cdot q \cdot 6.02 \times 10^{23}} \times 18 \quad (15)$$

The chemical energy output of the system is:

$$P_{che} = \frac{I_{cat}}{2q \cdot 6.02 \times 10^{23}} \Delta G_{ref} \quad (16)$$

### 3.3. Thermodynamic model

The remaining solar energy is absorbed on the surface of the absorber tube and converted into thermal energy, which could be calculated by:

$$P_{sol,abs} = \left(P_{sol} \cdot \gamma \cdot \alpha_{gla} - P_{sol,cat}\right) \cdot \alpha_{gla} \cdot \rho_{abs} \quad (17)$$

The mass flow rate of HTF in the absorber tube is

$$m_{HTF,abs} = \frac{P_{sol,abs}}{c_{p,HTF} \cdot (T_{out} - T_{in})} \quad (18)$$

where $c_{p,\,oil}$ is the specific heat capacity of HTF; $T_{in}$ and $T_{out}$ are the HTF temperatures at the inlet and outlet of the receiver, respectively.

A two-tank direct energy storage system is adopted, which is more efficient than a thermocline system and has the advantages of a simple structure and a high heat transfer efficiency [36,37]. The waste heat from storage tanks is considered negligible due to their high storage efficiency. In addition, the hot tank and cold tank temperatures are assumed to remain constant at $T_{hot}$ and $T_{cold}$ over time to provide a stable heat source for the system. The thermal energy stored in the TES process is

$$Q_{TES} = \left(m_{HTF,abs} - m_{HTF,eva} - m_{HTF,reh}\right) \cdot c_{p,HTF} \cdot (T_{hot} - T_{cold}) \times 3600 \quad (19)$$

where $m_{HTF,\,eva}$ is the HTF mass flow rate in solar evaporator; $T_{hot}$ and $T_{cold}$ are the HTF temperatures stored in hot and cold tank, which are assumed to be equal to $T_{out}$ and $T_{in}$, respectively.

To ensure the stability of the power generation load of the system, the mass flow rate of the HTF out of the hot tank should be constant in unit time. The mass balance equation of the hot and cold tank are

$$\frac{d(M_{hot})}{d\tau} = m_{HTF,abs} - m_{HTF,eva} - m_{HTF,reh} \quad (20)$$

$$\frac{d(M_{cold})}{d\tau} = m_{HTF,eva} + m_{HTF,reh} - m_{HTF,abs} \quad (21)$$

where $M_{hot}$ and $M_{cold}$ are the mass of the HTF in the hot and cold tank, respectively, and $\tau$ is the unit time.

The energy balance equations for the TES process is

$$\frac{d(Q_{TES})}{d\tau} = P_{sol,abs} - m_{HTF,abs} \cdot c_{p,HTF} \cdot (T_{hot} - T_{cold}) - P_{rad1} \quad (22)$$

where $Q_{TES}$ is the real thermal energy stored in the TES process.

The heat flux in the photocatalytic layer is used to preheat the circulating water and increase the reaction temperature. One function of this heat flux is to increase the solar evaporator inlet temperature of the Rankine cycle, thus improving the electricity efficiency, and the other function is to reduce the Gibbs free energy of water splitting, thus improving the hydrogen production efficiency. The heat flux in photocatalytic layer can be calculated by:

$$P_{recy} = P_{non\text{-}rad} + P_{relax1} + P_{relax2} + P_{rad1} - P_{rad2} \quad (23)$$

where $P_{rad1}$ is radiation heat loss of the absorber tube, $P_{rad2}$ is radiation heat loss of the photocatalytic layer.

The thickness of the photocatalytic layer is negligible compared to that of the glass layer located below the catalyst, so the emissivity of the glass is assumed to be the overall emissivity of the catalyst and glass. The radiation heat loss of the absorber tube is:

$$P_{rad1} = A_{abs} \cdot \left[\frac{1}{\varepsilon_{abs}} + \frac{A_{abs}}{A_{cat}}\left(\frac{1}{\varepsilon_{gla}} - 1\right)\right]^{-1} \cdot \sigma \cdot \left(T_{abs}^4 - T_{cat}^4\right) \quad (24)$$

where $\varepsilon_{abs}$ and $\varepsilon_{cat}$ are the emittance of the absorber tube and photocatalytic layer, respectively, σ is the Stefan-Boltzmann constant, $T_{abs}$ is the temperature of absorber tube, which is set 5 °C higher than $T_{out}$.

The radiation heat loss of the photocatalytic layer is:

$$P_{rad2} = A_{cat} \cdot \left[\frac{1}{\varepsilon_{gla}} + \frac{A_{cat}}{A_{gla}}\left(\frac{1}{\varepsilon_{gla}} - 1\right)\right]^{-1} \cdot \sigma \cdot \left(T_{cat}^4 - T_{ref}^4\right) \quad (25)$$

where $A_{gla}$ is the area of the glass tube, $\varepsilon_{gla}$ is the emittance of the glass tube, $T_{ref}$ is the temperature at the reference point.

The heat flux in the photocatalytic layer may not be sufficient to convert water into steam due to the high latent heat of water vaporization. Moreover, further increasing the steam pressure to meet the demand of the turbine inlet pressure is difficult. Thus, the photocatalysis reaction occurs in a liquid-phase environment. The energy balance equations in the evaporator, reheater and photocatalytic layer can be described by:

$$m_{HTF,abs} \cdot c_{p,HTF} \cdot (T_{hot} - T_{cold}) = m_w \cdot (h_6 - h_3) + m_w \cdot (h_8 - h_7) \quad (26)$$

$$P_{recy} = (1 - \beta) \cdot m_w \cdot \left(h_{cat,out} - h_{11}\right) + m_{sup1} \cdot \left(h_{cat,out} - h_{ref}\right) \quad (27)$$

where $m_w$ is the mass flow rate of the water in Rankine cycle; $m_{sup1}$ is the mass flow rate of the supply water from the tank of water supply 1; $h_5$ and $h_6$ are are the enthalpy of the working fluid at the solar evaporator outlet and inlet, respectively; $h_{11}$ and $h_{cat,\,out}$ are the enthalpy of the working fluid at the pump 2 and photocatalytic layer outlet, respectively. $h_{ref}$ is the enthalpy at the reference point.

The mass balance equation in photocatalytic layer can be described by:

$$m_{sup1}(T_{amb}) + m_{sup2}(T_{amb}) = m_{con} + m_{hw} \quad (28)$$

The system power output mainly consists of the HPT and LPT, and the power consumption mainly includes pump 1 and pump 2. Thus, the net power outputs for the systems can be expressed as

$$P_{ele} = \sum P_T - \sum P_{FP} = P_{HPT} + P_{LPT} - P_{P1} - P_{P2} \quad (29)$$

where $P_{HPT}$ is the high-pressure turbine power output, $P_{LPT}$ is the low-pressure turbine power output, $P_{P1}$ is the power consumed by pump 1, $P_{P2}$ is the power consumed by pump 2.

The $h_2$ is calculated by:

$$h_2 = \frac{m_{sup1} \cdot h_{ref} + (1 - \beta) \cdot m_w \cdot h_{11} - m_{con} \cdot h_{cat,out} - m_{hw} \cdot h_{cat,out} + m_{sup2} \cdot h_{ref}}{m_w} \quad (30)$$

When the heat load of the solar evaporator and reheater changes, the mass flow rate of the water changes. Therefore, the isentropic efficiency of the turbines and pumps in the system will be influenced. An empirical

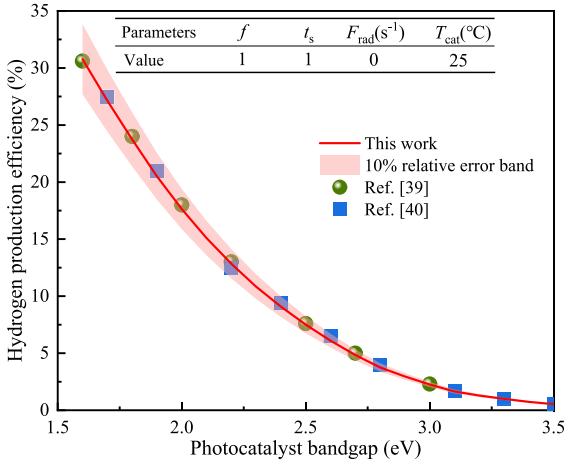


(a) Verification of the solar photocatalytic model with Ref. [40] and Ref. [40]

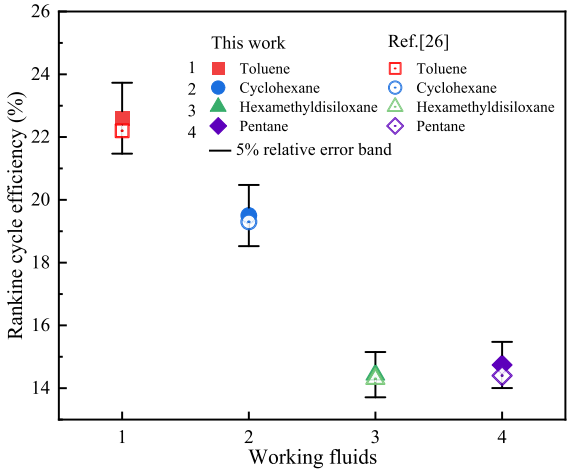


(b) Verification of the Rankine cycle model with Ref. [40]

**Fig. 5.** Verification of the solar photocatalytic model and Rankine cycle model. (a) Verification of the solar photocatalytic model with Ref. [40] and Ref. [41] (b) Verification of the Rankine cycle model with Ref. [27]

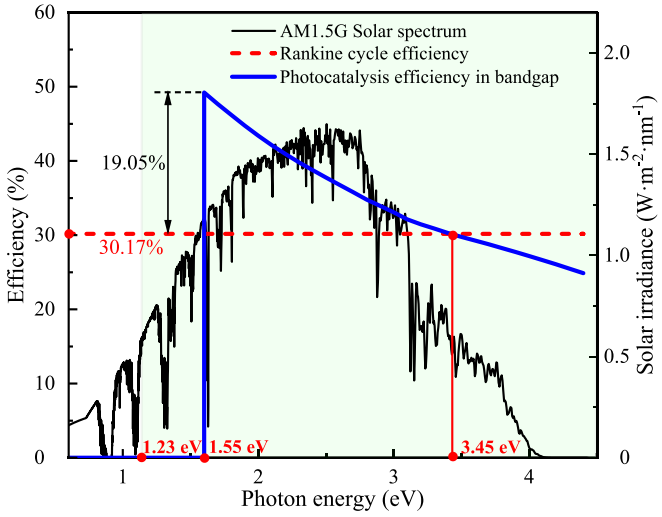


**Fig. 6.** Solar photon utilization efficiency of photocatalysis water splitting process and steam Rankine cycle.

formula is used to correct the isentropic efficiency of the turbines and pumps [38,39].

$$\frac{\eta_{is,T}}{\eta_{is,T,d}} = -1.0176\left(\frac{m}{m_d}\right)^4 + 2.443\left(\frac{m}{m_d}\right)^3 - 2.1812\left(\frac{m}{m_d}\right)^2 + 1.0535\left(\frac{m}{m_d}\right) + 0.701 \tag{31}$$

$$\frac{\eta_{is,P}}{\eta_{is,P,d}} = -0.44\left(\frac{V}{V_d}\right)^3 + 0.47\left(\frac{V}{V_d}\right)^2 + 0.45\left(\frac{V}{V_d}\right) + 0.52 \tag{32}$$

where $\eta_{is,\,T,\,d}$ and $\eta_{is,\,P,\,d}$ are the turbine and pump designate isentropic efficiency, respectively; $\eta_{is,\,T}$ and $\eta_{is,\,P}$ are the turbine and pump real isentropic efficiency; $m/\,m_d$ is the steam mass flow ratio comparing with the designate condition; $V/\,V_d$ is the volume flow ratio comparing with the designate condition.

### 3.4. System evaluation model

The chemical energy conversion efficiency is used to evaluate the photocatalytic hydrogen production performance, which is expressed as:

$$\eta_{che} = \frac{P_{che}}{P_{sol}} \tag{33}$$

The electricity efficiency is used to evaluate the Rankine cycle power generation performance, which is expressed as:

$$\eta_{ele} = \frac{P_{ele}}{P_{sol}} \tag{34}$$

Since hot water can be produced from the photocatalytic layer, the exergy efficiency is used to evaluate the hot water.

$$\eta_{ex,hw} = \frac{Ex_{hw}}{Ex_{sol}} \tag{35}$$

And the system total exergy efficiency is:

$$\eta_{ex,sys} = \eta_{che} + \eta_{ele} + \eta_{ex,hw} \tag{36}$$

The reference point is taken as 298.15 K, 101.325 kPa, and the exergy of the state point $i$ is:

$$Ex_i = m_i \cdot \left[h_i - h_{ref} - T_{ref}\left(s_i - s_{ref}\right)\right] \tag{37}$$

### 3.5. Validation of the calculation model

To verify the reliability of the model used in this study, the photocatalysis case in Ref. [40] as well as Ref. [41] and the Rankine cycle case in Ref. [27] are chosen as research case studies. The solar photocatalytic model and Rankine cycle model verification results are shown in Fig. 5 (a) and Fig. 5 (b), respectively. The results agree well with those in the literature.

## 4. Results and discussion

In this section, the efficiencies of solar photon utilization through photocatalysis and the Rankine cycle are compared. Then, the optical and heat losses in the proposed receiver (PR) and conventional receiver (CR) are analyzed. The system efficiency is also studied with and without preheating of the circulating water by the heat flux of the photocatalytic layer. Additionally, the energy flow under the design conditions is addressed. Finally, a strategy for full-condition operation of the system is developed, and the system performance on typical days and throughout the year is investigated.

### 4.1. Performance of the solar conversion process

The solar photon utilization efficiencies of photocatalytic water

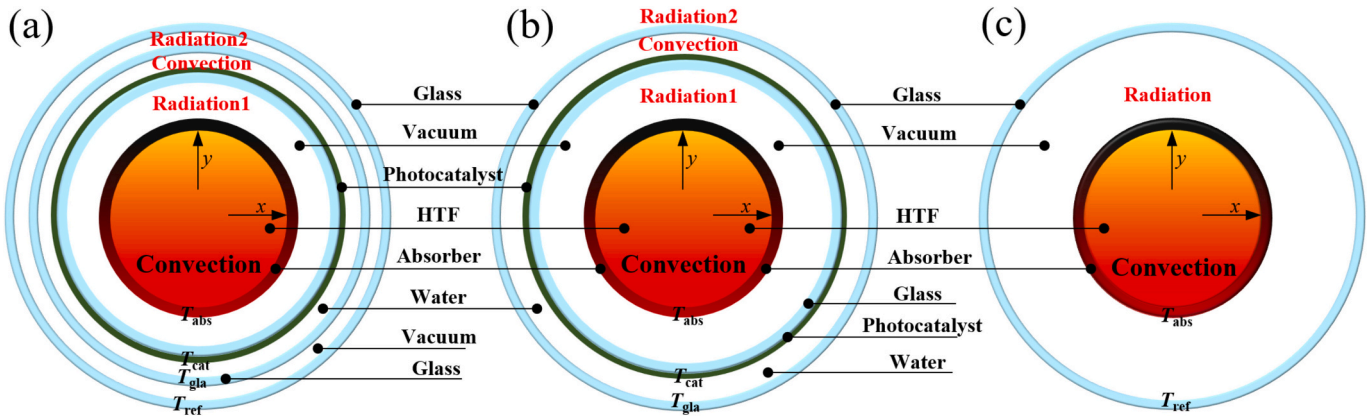


**Fig. 7.** Schematic diagram of the receiver with (a) proposed receiver1 (PR1), (b) proposed receiver1 (PR2), and (c) the conventional receiver (CR).

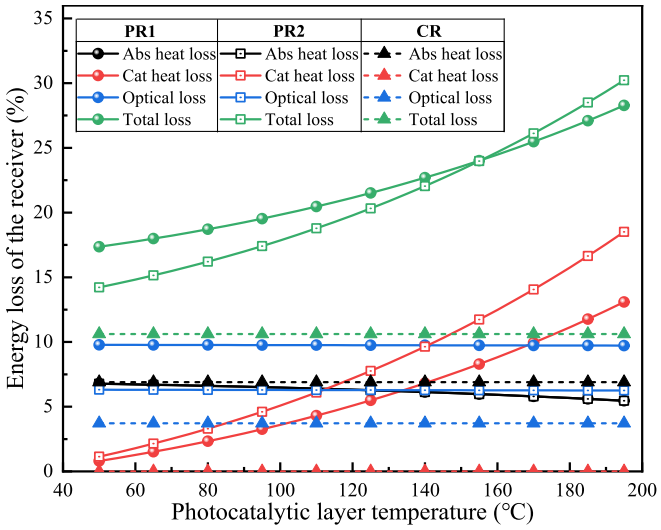


**Fig. 8.** Heat and optical loss of the PR1, PR2 and CR at different temperature of the catalyst layer.

splitting for hydrogen production in the bandgap and the steam Rankine cycle in the proposed system are shown in Fig. 6. For solar energy, from the perspective of engineering thermodynamics, the solar photon energy differs in quality at different wavelengths. For the Rankine cycle, all photons are converted into thermal energy, and the cycle efficiency is independent of the photon energy at a specific wavelength. Therefore, the cycle efficiency is constant over the entire wavelength range and is 30.17 % in the proposed system. For the photocatalytic water splitting reaction, the energy barrier of water splitting limits the utilization of the solar spectrum as well as photons with different energies. In addition, the number of effective EHPs is limited by recombination and relaxation. This leads to the need to operate the water splitting reaction, which has an energy barrier of 1.23 eV, at an overpotential of 1.55 eV, as shown in Fig. 6. The photocatalytic reaction efficiency ranges from 0 to 19.05 % higher than that of the Rankine cycle when the photocatalyst bandgap is in the range of 1.55 to 3.45 eV. In contrast, the solar photon utilization efficiency of photocatalysis is less than that of the Rankine cycle when the photocatalyst bandgap is greater than 3.45 eV because the photon energy above the Gibbs free energy barrier is dissipated as heat, which is the main source of thermalization loss. Nevertheless, the stored energy of the reaction remains constant [40]. The greater the photon energy is, the greater the relaxation loss from the photocatalytic reaction. Accordingly, although the Rankine cycle can utilize full-spectrum photons, the selection of appropriate photocatalysts can enhance the full-spectrum utilization efficiency to achieve the incorporation of the photocatalysis process and Rankine cycle.

Both the PR and the CR are displayed in Fig. 7. PR1 has three layers of glass, which are used to support the photocatalyst, act as a reaction chamber, and reduce the radiative thermal loss in order from inside to outside. In contrast, PR2 has no glass layer for thermal insulation, and the outer glass layer radiatively transfers heat to the environment and is assumed to be at the same temperature as the reaction temperature.

The optical and heat losses of the receivers are compared, which mainly include the glass tube optical loss, absorber tube radiation heat loss and photocatalytic layer radiation heat loss, as shown in Fig. 7. Fig. 8 shows that the heat loss of the absorber tube in PR1 and PR2, which ranges from 5.46 % to 6.77 %, slightly increases with increasing photocatalytic layer temperature but is always lower than that of CR (6.90 %), indicating that the photocatalytic layer plays a role similar to that of a radiation shield layer [25], thus reducing the radiation heat loss of the absorber tube. Furthermore, the heat loss of the absorber tube in

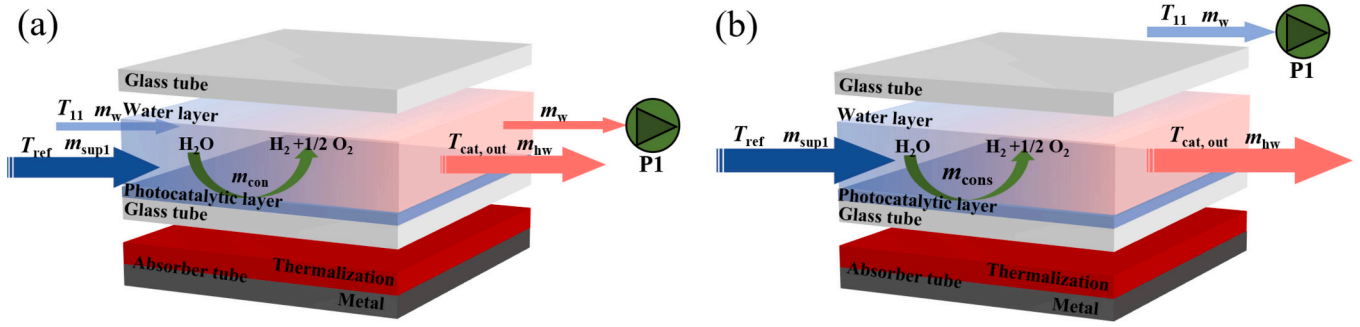


**Fig. 9.** Schematic diagram of two cycle process with (a) preheating the circulating water (PCW), and (b) non-preheating the circulating water (NPCW) by the heat flux of the photocatalytic layer.

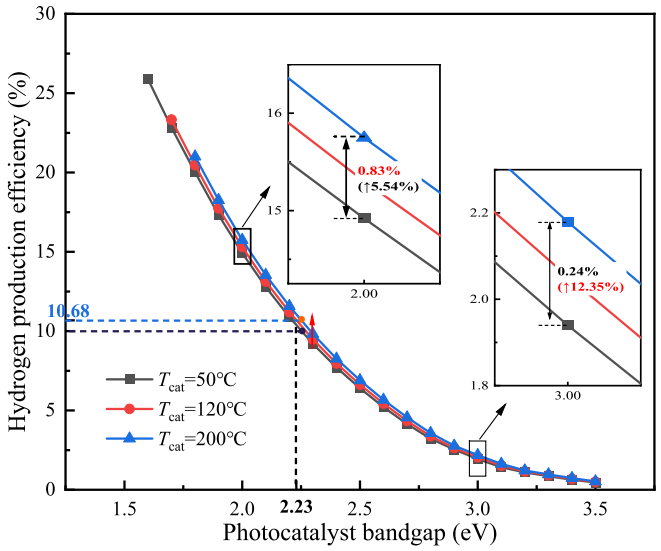


(a) Effects on hydrogen production efficiency

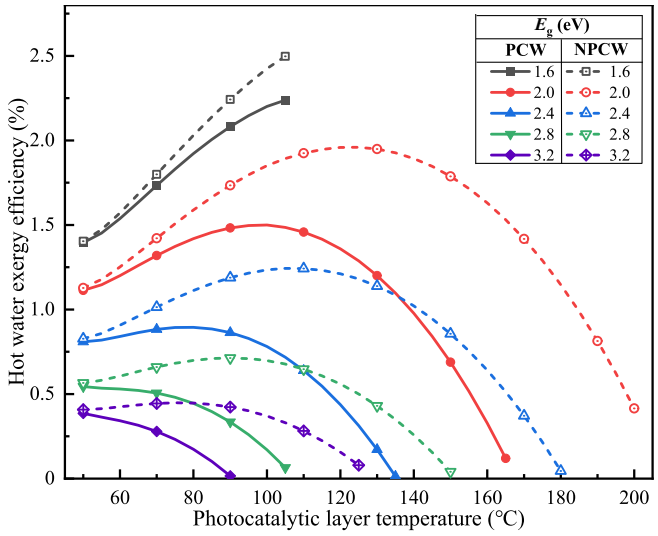


(c) Effects on hot water exergy efficiency

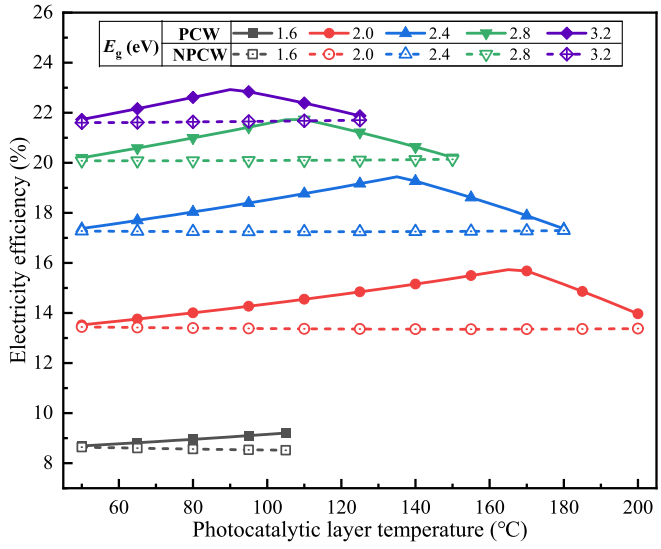


(b) Effects on electricity generation efficiency

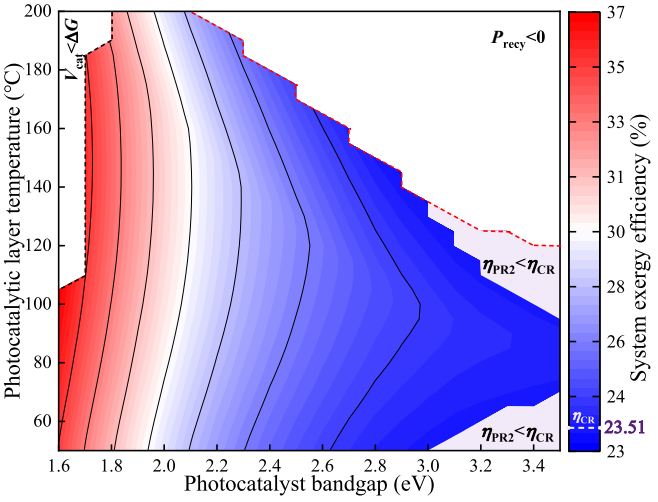


(d) Effects on system exergy efficiency

**Fig. 10.** Effects of temperature and bandgap of photocatalyst on system performance.

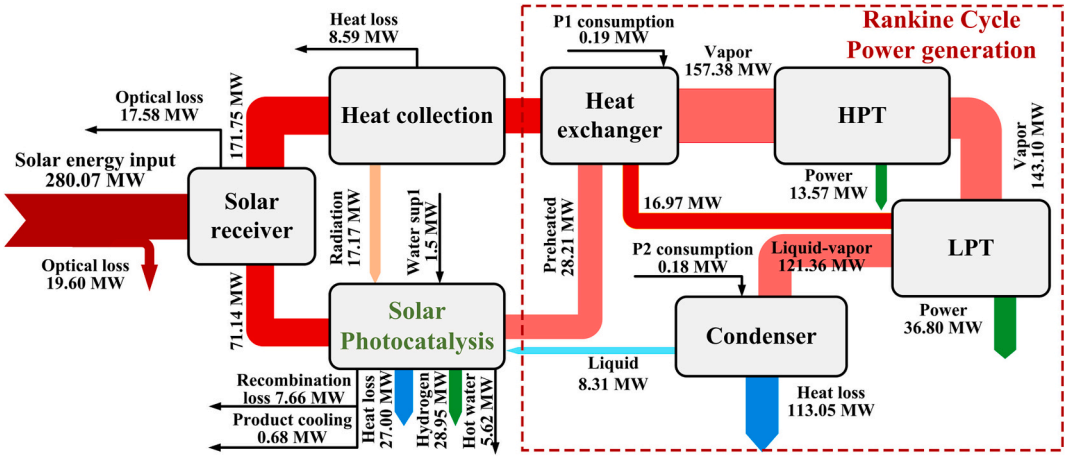


**Fig. 11.** Energy flow diagram of the proposed system under the design condition.

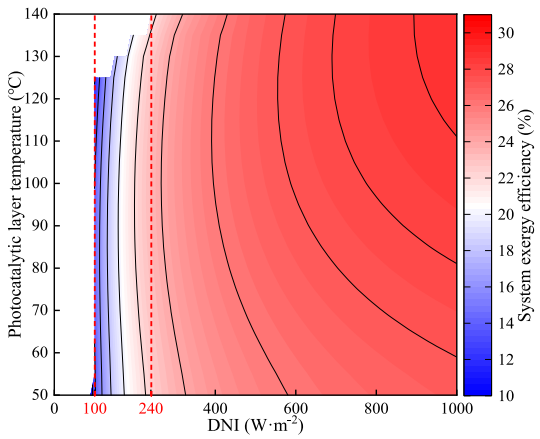


(a) Photocatalytic layer temperature analysis according to the variation in the DNI

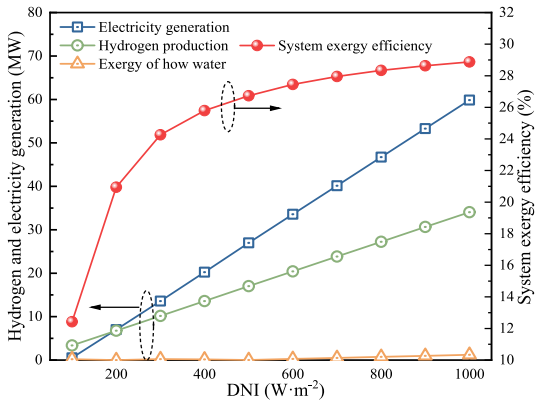


(b) System performance under each DNI

**Fig. 12.** System parameter analysis based on exergy efficiency and performance analysis.

PR1 and PR2 could be reutilized in the photocatalytic layer to preheat the circling water of the Rankine cycle. However, a higher temperature can increase the heat loss of the photocatalytic layer. The influence of temperature on the heat loss of the photocatalytic layer is more pronounced at higher temperatures and even reaches 13.08 % and 18.51 % for PR1 and PR2, respectively. Although PR1 can reduce the heat loss compared to PR2, the increase in the number of glass layers will result in more optical losses. Therefore, the equilibrium point for the photocatalytic layer temperature is 155 °C, at which the total energy losses of PR1 and PR2 are the same. Compared with PR1, PR2 has relatively high efficiency at temperatures below 160 °C. Overall, although the results indicate that both PR1 and PR2 bring about more optical and heat losses than CR, the efficiency gains from the addition of the photocatalytic layer outweigh the energy losses caused by PR1 and PR2, as shown in the next analysis. Considering the total loss of the receiver and commercial costs, PR2 is adopted and used in the proposed system and subsequent calculations.

### 4.2. *Effect of the photocatalyst bandgap and temperature*

The heat flux within the photocatalyst, which is closely related to the bandgap and surface temperature, mainly arises from relaxation and non-radiative recombination of EHPs as well as radiation heat loss from the absorber tube. The heat flux is used to preheat the water. In this work, the two cases of whether preheated water is used for the Rankine cycle are compared, as shown in Fig. 9. The effects of the photocatalyst bandgap and temperature on the system efficiency are analyzed, as shown in Fig. 10.

Fig. 10 (a) illustrates that the hydrogen production efficiency increases with increasing photocatalyst temperature, from 10 % at 50 °C to 10.65 % at 200 °C, with a bandgap of 2.23 eV. This result indicates that the beneficial effect of increasing the temperature on the chemical reaction and spectral absorption of the catalyst exceeds the negative effect on EHP recombination. Furthermore, the improvement ratio of the hydrogen production efficiency decreases with increasing bandgap, with values of 0.83 % at 2.0 eV and 0.24 % at 3.0 eV when the temperature increases from 50 °C to 200 °C.

According to Fig. 10 (b), the electricity efficiency of the CPC process is always superior to that of the CNPC process since the extremely high inlet temperature of the solar evaporator improves the Rankine cycle efficiency. In both processes, the electricity efficiency improves with increasing bandgap, as more solar energy is injected into the Rankine cycle. Additionally, the electricity efficiency of the CPC process peaks when the photocatalyst temperature increases and the bandgap is

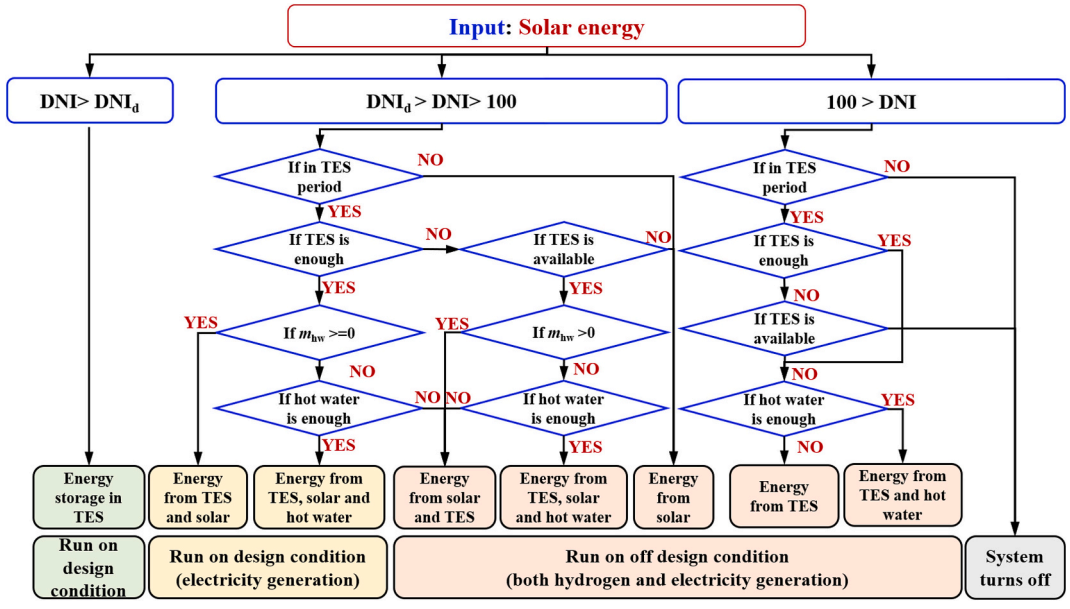


**Fig. 13.** Off-design condition operational simulation strategy for the proposed system.

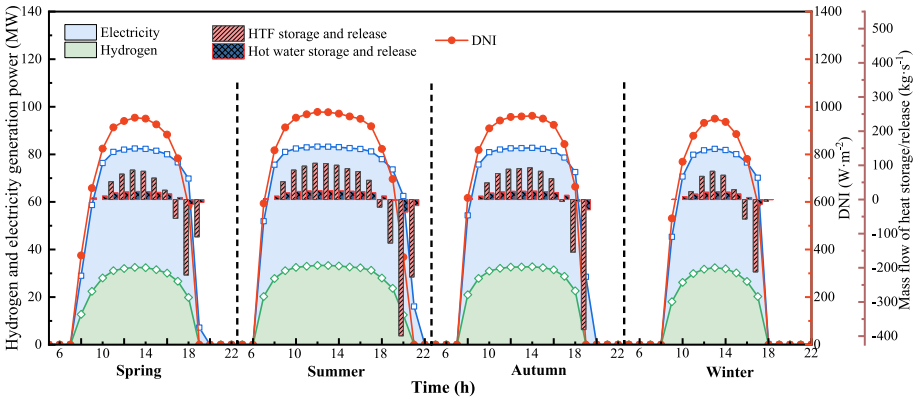


(a) Electricity and hydrogen generation as well as heat storage and release performance

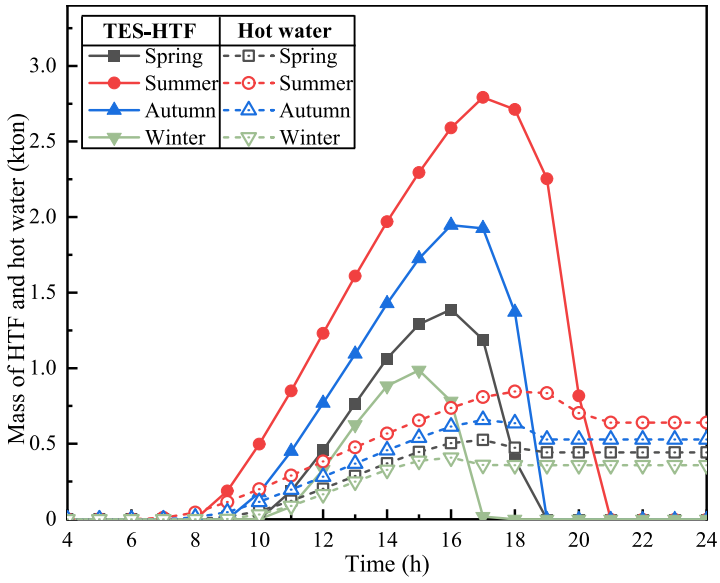


(b) Cumulative mass of HTF and hot water in the hot tank and hot water tank

**Fig. 14.** System daily performance analysis within the typical days.

greater than 1.7 eV. Furthermore, as the bandgap widens, the peak temperature moves to lower temperatures, reaching 165 °C at 2.0 eV and 90 °C at 3.2 eV. The main reason is that when the heat flux in the photocatalytic layer is sufficient to completely preheat the circulating water, the electricity efficiency improves with increasing evaporator inlet temperature. When the heat is insufficient, the continuous increase in temperature increases the radiation heat loss from the photocatalytic layer, leading to more radiation heat loss, as shown in Fig. 8. Therefore, the heat that can be reutilized by the Rankine cycle decreases, and the electricity efficiency decreases.

As shown in Fig. 10 (b) and Fig. 10 (c), the peak electricity efficiency is achieved when the photocatalyst is exactly completely preheating the circulating water. Eventually, the CPC process harvests more electricity and achieves greater exergy efficiency than the CNPC process. Additionally, the system exergy efficiency with PR2 is consistently greater than that with CR (23.51 %) for bandgaps below 2.9 eV, as shown in Fig. 10 (d). Otherwise, the improvement in efficiency from chemical reactions is lower than the energy loss from added catalytic and glass layers.

Considering the efficiency of commercially available hydrogen production, a solar-to-hydrogen efficiency of 10 % is adopted as the designated condition [42], corresponding to 2.23 eV. Based on the overall energy balance, a higher utilization of heat dissipated from the photocatalytic layer to preheat the circulating water means a reduced HTF mass flow rate, and the high cost of solar field installation can thus be minimized. In addition, an appropriate temperature for the photocatalytic layer is necessary for reducing the heat loss and increasing the system exergy efficiency. As shown in Fig. 10 (d), the optimal photocatalyst temperature of 140 °C with a bandgap of 2.23 eV is adopted as the designated operating parameters.

### 4.3. Performance of the proposed system

The energy flow of the proposed system under the design conditions is shown in Fig. 11. The total solar energy input is 280.07 MW. After an optical loss of 37.18 MW via the mirror and glass tube, 71.14 MW passes through the photocatalytic layer, and the remaining 171.75 MW passes through the absorber tube. The main energy losses of the system are heat loss, optical loss and EHP loss. The total heat loss of the system is 14.32 MW, which mainly includes the condenser heat loss, photocatalytic layer radiation heat loss, absorber tube collection heat loss and product cooling heat loss of 113 MW, 27 MW, 8.59 MW and 0.68 MW, respectively. The EHP loss includes excitation loss and non-radiative recombination, with a total value of 7.66 MW. Furthermore, the absorber tube

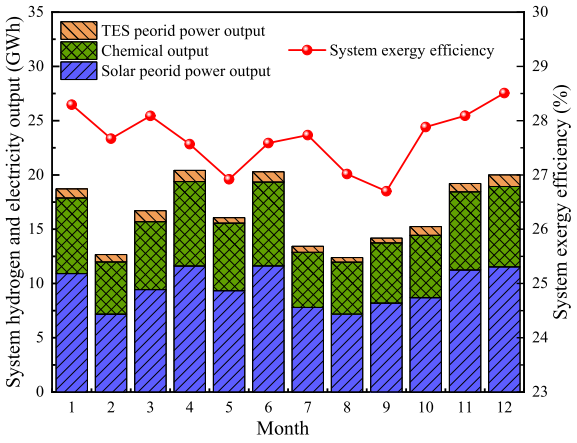


(a) Monthly hydrogen and electricity generation as well as exergy efficiency

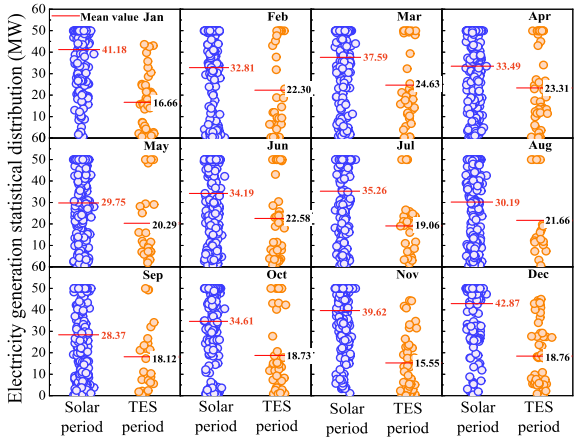


(b) Statistical distribution of electricity generation at solar and TES period

**Fig. 15.** System annual performance analysis.

radiation heat loss of 17.17 MW and heat dissipated in the photocatalytic layer of 9.23 MW are transferred to the water, after the photocatalytic radiation heat loss. Therefore, liquid circulating water from the outlet of P2 with an energy of 8.31 MW is preheated to 28.21 MW, and 5.62 MW is stored as hot water. Additionally, 50 MW and 28.95 MW of the input solar energy are converted into electricity and hydrogen by the Rankine cycle and photocatalysis, with efficiencies of 10.34 % and 17.85 %, respectively. Ultimately, the total exergy efficiency of the proposed system could be increased to 28.49 % under the design conditions compared to that of the conventional PTC thermal power system whose total exergy efficiency is mainly around 20 % [43,44]. Besides, the proposed system simultaneously achieves cogeneration of electricity, hydrogen and hot water.

The system performance under different solar energy inputs ranging from 0 to 1000 W·m$^{-2}$ is analyzed, and the photocatalytic layer temperature under different DNI values for corresponding maximum system exergy efficiency is investigated. Fig. 12 (a) illustrates that when the DNI is lower than 100 W·m$^{-2}$, the system exergy efficiency sharply decreases to 0. The main reason is that the absorber tube stops working when the amount of collected heat is less than the radiation heat loss, leading to the heat flux in the photocatalytic layer not being sufficient to increase the water to the designated temperatures. Moreover, when the DNI ranges from 100 W·m$^{-2}$ to 240 W·m$^{-2}$, the system still does not operate at the design temperature because of the insufficient heat flux from EHP relaxation and recombination in the photocatalytic layer. However, the proposed system can maintain the temperature and has the corresponding maximum system exergy efficiency when the DNI is greater than 240 W·m$^{-2}$. Additionally, Fig. 12 (b) shows the system electricity, hydrogen generation and exergy efficiency performance when system has the corresponding maximum exergy system efficiency under each DNI. As the DNI increases, the percentage of radiation heat loss from the system decreases, leading to a relatively stable system exergy efficiency within 25.80 % to 28.87 % when the DNI is greater than 400 W·m$^{-2}$.

Considering the changes in real solar energy input conditions and based on the system performance shown in Fig. 12, an off-design condition operational simulation strategy is proposed, as shown in Fig. 13, and the corresponding system performance is further investigated.

For the proposed system, based on the hourly meteorological conditions, four typical days (21st of March, 22nd of June, 22nd of September and 23rd of December) are selected. The detailed system performance is shown in Fig. 14. Fig. 14 (a) indicates that surplus thermal energy could be stored by the TES process and released to maintain the operational temperature of the Rankine cycle when the DNI deviates from the design conditions, which could improve the stability and running time. However, since the solar multiple is set to 1, the TES process has a limited heat storage capacity during typical days and only maintains the system under the design conditions for an average duration of 2.5 h. Moreover, an average surplus of 101.51 tons of hot water is stored, as shown in Fig. 14 (b).

The annual performance of the system is shown in Fig. 15 (a). The highest monthly electricity generation and hydrogen generation are 7.72 GWh-eq and 11.62 GWh, respectively, in April. However, the highest monthly system exergy efficiency of 28.51 % occurs in December, mainly due to the better turbine operational stability. Fig. 15 (b) shows the system electricity generation statistical distribution and mean power output in the solar and TES periods. The highest mean electricity generation occurs in December and March for the solar period and TES period, respectively. Overall, the solar ordered conversion system can achieve cogeneration of electricity, hydrogen and hot water, with annual average efficiencies of 10.32 %, 16.88 % and 0.47 %, respectively. In addition, the proposed system that couples photocatalysis with Rankine cycle processes can achieve a higher annual exergy efficiency of 27.67 % compared with the conventional solar Rankine cycle under off-design conditions.

## 5. Conclusion

In this work, a hybrid hydrogen and electricity cogeneration system driven by concentrated solar energy is proposed, which can utilize the full spectrum of solar energy in an orderly manner. The incorporation of photocatalysis for hydrogen production and the Rankine cycle could theoretically enhance the solar photon utilization efficiency when the photocatalyst bandgap is in the range of 1.55 to 3.45 eV. In addition, the photocatalytic layer in the PR plays a role similar to that of a radiation shield, reducing the radiation heat loss of the absorber tube from 6.90 % to 5.46 %. Furthermore, the dissipated heat of the EHPs and radiation heat loss of the absorber tube could be reutilized in the photocatalytic layer to preheat the circulating water to increase the hydrogen production efficiency (from 10 % to 10.34 %) and electricity generation efficiency (from 15.73 % to 17.85 %) under the design conditions. In addition, 28.95 MW, 50 MW and 5.62 MW of the input 280.07 MW of solar energy could be stored during the photocatalysis and Rankine cycle processes in the form of hydrogen, electricity and hot water, respectively. Generally, the total exergy efficiency of the proposed system could be increased compared to that of the conventional PTC thermal power system, from 23.51 % to 28.49 %. Then, the photocatalytic layer temperature of the proposed system is adjusted for the corresponding maximum exergy efficiency according to the variation in the DNI. The proposed system can maintain the designated temperature when the DNI is greater than 240 W·m$^{-2}$. When the DNI ranges from 100 W·m$^{-2}$ to 240 W·m$^{-2}$, the photocatalytic layer temperature needs to be adjusted to achieve the corresponding maximum system exergy efficiency. Finally, the system annual average exergy efficiency is 27.67 % under off-design

conditions.

To further improve the simulation accuracy of the system proposed in this work, experiments will be conducted and the key parameters in the model will be corrected based on the experimental results. According to the work, fabricating excellent photocatalytic film with good transmittance and quantum efficiency, building receivers which conclude photocatalytic layer and heat collection tube, and conducting experiments under real sunlight will be the key points for achieving full-spectrum solar energy utilization in the future.

## CRediT authorship contribution statement

**Entao Zhang:** Writing – review & editing, Writing – original draft, Software, Methodology, Investigation, Formal analysis, Data curation. **Chenyu Xu:** Writing – review & editing, Supervision, Funding acquisition, Conceptualization. **Yuan Gao:** Supervision, Methodology, Data curation. **Xuan Zhu:** Resources, Investigation, Data curation. **Yin Xie:** Resources, Investigation, Data curation. **Mingpan Xu:** Investigation, Data curation. **Yanwei Zhang:** Writing – review & editing, Supervision, Funding acquisition, Conceptualization.

## Declaration of competing interest

The authors declare that they have no known competing financial interests or personal relationships that could have appeared to influence the work reported in this paper.

## Data availability

Data will be made available on request.

## Acknowledgements

This work was supported by the National Natural Science Foundation of China (52341602), the Zhejiang Provincial Natural Science Foundation of China under Grant (No. LDT23E06014E06), the Zhejiang Provincial Natural Science Foundation of China under Grant (No. LQ24E060001), the National Key Research and Development Project (2023YFC3710800) and the Fundamental Research Funds for the Central Universities (2022ZFJH04).

## References

[1] Gernaat DEHJ, De Boer HS, Daioglou V, Yalew SG, Müller C, Van Vuuren DP. Climate change impacts on renewable energy supply. Nat Clim Chang 2021;11(2):119–25.
[2] Bolsen T. Framing renewable energy. Nat Energy 2022;7(11):1003–4.
[3] Hong JN, Xu CY, Deng BW, Gao Y, Zhu X, Zhang XH, et al. Photothermal chemistry based on solar energy: from synergistic effects to practical applications. Adv Sci 2022;9(3):2103926.
[4] Gong J, Li C, Wasielewski MR. Advances in solar energy conversion. Chem Soc Rev 2019;48(7):1862–4.
[5] Fang J, Wu H, Liu T, Zheng Z, Lei J, Liu Q, et al. Thermodynamic evaluation of a concentrated photochemical–photovoltaic–thermochemical (CP-PV-T) system in the full-spectrum solar energy utilization. Appl Energy 2020;279:115778.
[6] Cheng W-H, Richter MH, May MM, Ohlmann J, Lackner D, Dimroth F, et al. Monolithic Photoelectrochemical device for direct water splitting with 19% efficiency. ACS Energy Letters 2018;3(8):1795–800.
[7] Geisz JF, France RM, Schulte KL, Steiner MA, Norman AG, Guthrey HL, et al. Six-junction III–V solar cells with 47.1% conversion efficiency under 143 suns concentration. Nat Energy 2020;5(4):326–35.
[8] Wang Q, Pornrungroj C, Linley S, Reisner E. Strategies to improve light utilization in solar fuel synthesis. Nat Energy 2022;7(1):13–24.
[9] Shockley W, Queisser HJ. Detailed balance limit of efficiency of p-n junction solar cells. J Appl Phys 1961;32(3):510–9.
[10] Xu N, Zhu P, Sheng Y, Zhou L, Li X, Tan H, et al. Synergistic tandem solar electricity-water generators. Joule 2020;4(2):347–58.
[11] Herrando M, Wang K, Huang G, Otanicar T, Mousa OB, Agathokleous RA, et al. A review of solar hybrid photovoltaic-thermal (PV-T) collectors and systems. Prog Energy Combust Sci 2023;97:101072.
[12] Weinstein LA, Mcenaney K, Strobach E, Yang S, Bhatia B, Zhao L, et al. A hybrid electric and thermal solar receiver. Joule 2018;2(5):962–75.
[13] Zhu L, Yang W, Pan H, Shao Z, Lu Y, Dang Z-M. Coupling the full solar spectrum with a two-step thermo-electrolytic cycle for efficient solar hydrogen production. Energy Convers Manag 2023;290:117161.
[14] Bermel P, Yazawa K, Gray JL, Xu X, Shakouri A. Hybrid strategies and technologies for full spectrum solar conversion. Energy Environ Sci 2016;9(9):2776–88.
[15] Robertson J, Riggs B, Islam K, Ji YV, Spitler CM, Gupta N, et al. Field testing of a spectrum-splitting transmissive concentrator photovoltaic module. Renew Energy 2019;139:806–14.
[16] Pinaud BA, Benck JD, Seitz LC, Forman AJ, Chen Z, Deutsch TG, et al. Technical and economic feasibility of centralized facilities for solar hydrogen production via photocatalysis and photoelectrochemistry. Energy Environ Sci 2013;6(7):1983–2002.
[17] Holmes-Gentle I, Tembhurne S, Suter C, Haussener S. Kilowatt-scale solar hydrogen production system using a concentrated integrated photoelectrochemical device. Nat Energy 2023;8(6):586–96.
[18] Zhang T, Guan X, Zhang Z, Wang B, Qu J, Zeng W, et al. Photothermal catalytic hydrogen production coupled with thermoelectric waste heat utilization and thermal energy storage for continuous power generation. Nano Energy 2024;121:109273.
[19] Gopinath CS, Nalajala N. A scalable and thin film approach for solar hydrogen generation: a review on enhanced photocatalytic water splitting. J Mater Chem A 2021;9(3):1353–71.
[20] Pornrungroj C, Andrei V, Reisner E. Thermoelectric–Photoelectrochemical Water Splitting under Concentrated Solar Irradiation. J Am Chem Soc 2023;145(25):13709–14.
[21] Guo Y, Chen J, Song H, Zheng K, Wang J, Wang H, et al. A review of solar thermochemical cycles for fuel production. Appl Energy 2024;357:122499.
[22] Bierman DM, Lenert A, Wang EN. Spectral splitting optimization for high-efficiency solar photovoltaic and thermal power generation. Appl Phys Lett 2016;109(24):243904.
[23] Moreno-Tejera S, Silva-Pérez MA, Lillo-Bravo I, Ramírez-Santigosa L. Solar resource assessment in Seville, Spain. Statistical characterisation of solar radiation at different time resolutions. Sol Energy 2016;132:430–41.
[24] Gutiérrez RE, Haro P, Gómez-Barea A. Techno-economic and operational assessment of concentrated solar power plants with a dual supporting system. Appl Energy 2021;302:117600.
[25] Wang Q, Shen B, Huang J, Yang H, Pei G, Yang H. A spectral self-regulating parabolic trough solar receiver integrated with vanadium dioxide-based thermochromic coating. Appl Energy 2021;285:116453.
[26] Li Q, Zhang Y, Wen Z-X, Qiu Y. An evacuated receiver partially insulated by a solar transparent aerogel for parabolic trough collector. Energy Convers Manag 2020;214:112911.
[27] Yang J, Li J, Yang Z, Duan Y. Thermodynamic analysis and optimization of a solar organic Rankine cycle operating with stable output. Energy Convers Manag 2019;187:459–71.
[28] Wang Z, Hisatomi T, Li R, Sayama K, Liu G, Domen K, et al. Efficiency accreditation and testing protocols for particulate Photocatalysts toward solar fuel production. Joule 2021;5(2):344–59.
[29] Gong L, Zhang Y, Bai Z. Geothermal-solar hybrid power with the double-pressure evaporation arrangement and the system off-design evaluation. Energy Convers Manag 2021;244:114501.
[30] Meng D, Liu Q, Ji Z. Performance analyses of regenerative organic flash cycles for geothermal power generation. Energy Convers Manag 2020;224:113396.
[31] Meng D, Liu Q, Ji Z. Effects of two-phase expander on the thermoeconomics of organic double-flash cycles for geothermal power generation. Energy 2022;239:122346.
[32] Sun J, Liu Q, Duan Y. Effects of evaporator pinch point temperature difference on thermo-economic performance of geothermal organic Rankine cycle systems. Geothermics 2018;75:249–58.
[33] Zhang L, Zhang J, Yu H, Yu J. Emerging S-scheme Photocatalyst. Adv Mater 2022;34(11):2107668.
[34] Pässler R. Parameter sets due to fittings of the temperature dependencies of fundamental bandgaps in semiconductors. Phys Status Solidi B 1999;216(2):975–1007.
[35] Ghoussoub M, Xia MK, Duchesne PN, Segal D, Ozin G. Principles of photothermal gas-phase heterogeneous CO2 catalysis. Energy Environ Sci 2019;12(4):1122–42.
[36] Cocco D, Serra F. Performance comparison of two-tank direct and thermocline thermal energy storage systems for 1MWe class concentrating solar power plants. Energy 2015;81:526–36.
[37] Alvi JZ, Feng Y, Wang Q, Imran M, Alvi J. Modelling, simulation and comparison of phase change material storage based direct and indirect solar organic Rankine cycle systems. Appl Therm Eng 2020;170:114780.
[38] Zhang G, Zheng J, Yang Y, Liu W. Thermodynamic performance simulation and concise formulas for triple-pressure reheat HRSG of gas–steam combined cycle under off-design condition. Energy Convers Manag 2016;122:372–85.

[39] Mondejar ME, Ahlgren F, Thern M, Genrup M. Quasi-steady state simulation of an organic Rankine cycle for waste heat recovery in a passenger vessel. Appl Energy 2017;185:1324–35.
[40] Zhu Z, Liu X, Bao C, Zhang K, Song C, Xuan Y. How efficient could photocatalytic CO2 reduction with H2O into solar fuels be? Energy Convers Manag 2020;222:113236.
[41] Fountaine KT, Lewerenz HJ, Atwater HA. Efficiency limits for photoelectrochemical water-splitting. Nat Commun 2016;7(1):13706.
[42] Pihosh Y, Nandal V, Higashi T, Shoji R, Bekarevich R, Nishiyama H, et al. Tantalum nitride-enabled solar water splitting with efficiency above 10%. Adv Energy Mater 2023;13(36):2301327.
[43] Shahabuddin M, Alim MA, Alam T, Mofijur M, Ahmed SF, Perkins G. A critical review on the development and challenges of concentrated solar power technologies. Sustain Energy Technol Assess 2021;47:101434.
[44] Dowling AW, Zheng T, Zavala VM. Economic assessment of concentrated solar power technologies: a review. Renew Sust Energ Rev 2017;72:1019–32.